NANO LETTERS

Letter

pubs.acs.org/NanoLett

Silica Nanoparticles as Substrates for Chelator-free Labeling of Oxophilic Radioisotopes

Travis M. Shaffer,[†,‡,§,#] Matthew A. Wall,[†,‡,#] Stefan Harmsen,[†] Valerie A. Longo,[†] Charles Michael Drain,[‡] Moritz F. Kircher,*[,†,∥,⊥] and Jan Grimm*[,†,§,∥,⊥,▽]

[†]Department of Radiology, Memorial Sloan Kettering Cancer Center, New York, New York 10065, United States

[‡]Department of Chemistry, Hunter College of the City University of New York, New York, New York 10065, United States

[§]Molecular Pharmacology and Chemistry Program and [∥]Center for Molecular Imaging and Nanotechnology, Memorial Sloan Kettering Cancer Center, New York, New York 10065, United States

[⊥]Department of Radiology, Weill Cornell Medical College, New York, New York 10065, United States

[▽]Department of Pharmacology, Weill Cornell Medical College, New York, New York 10065, United States

Supporting Information

ABSTRACT: Chelator-free nanoparticles for intrinsic radiolabeling are highly desirable for whole-body imaging and therapeutic applications. Several reports have successfully demonstrated the principle of intrinsic radiolabeling. However, the work done to date has suffered from much of the same specificity issues as conventional molecular chelators, insofar as there is no singular nanoparticle substrate that has proven effective in binding a wide library of radiosotopes. Here we present amorphous silica nanoparticles as general substrates for chelator-free radiolabeling and demonstrate their ability to bind six medically relevant isotopes of various oxidation states with high radiochemical yield. We provide strong evidence that the stability of the binding correlates with the hardness of the radioisotope, corroborating the proposed operating principle. Intrinsically labeled silica nanoparticles prepared by this approach demonstrate excellent in vivo stability and efficacy in lymph node imaging.

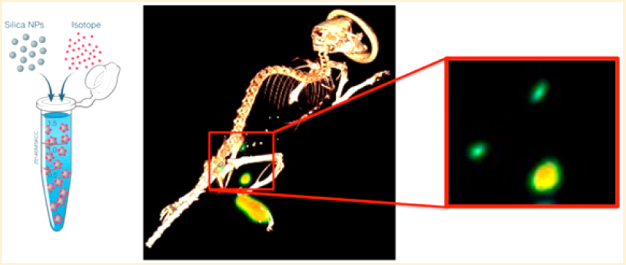

KEYWORDS: *Intrinsic labeling, chelator-free, radionuclide, silica nanoparticle, nuclear imaging, lymph node*

Nanoparticles possess several desirable features for use in disease imaging and therapy.[1−4] They can act as platforms for loading therapeutics and contrast agents while simultaneously anchoring targeting ligands or stealth polymer coatings.[5−7] Their size and surface chemistry can be tuned such that they exhibit attractive biological properties, such as passive accumulation and retention in cancer, in contrast to the rapid washout often observed by small molecular imaging agents.[8−10]

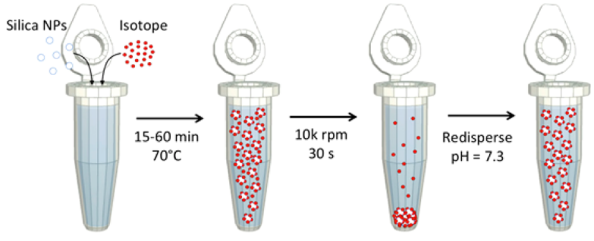

Figure 1. Scheme for intrinsic radiolabeling of silica nanoparticles. The nanoparticles are incubated with free radioisotope at 70 °C for 15 to 60 min depending on the specific radionuclide, then purified by centrifugation and resuspension.

Among the many imaging modalities that have adopted nanoparticle-based contrast agents, positron emission tomography (PET) and single-photon emission computed tomography (SPECT) have received considerable attention for their important roles in enabling whole-body imaging and pharmacokinetic studies.[11−13] Consequently, radiolabeled nanoparticles are of great interest to the nuclear imaging and nanooncology communities.

Radiolabeling of nanoparticles has primarily been achieved via surface functionalization of small molecular chelating agents that bind specific radioisotopes.[14] This approach enables utilization of labeling protocols that have already been established in molecular chelator research but presents several well-known disadvantages. Because the coordination chemistry of different isotopes varies greatly, there is no molecular chelator that can effectively bind many radioisotopes interchangeably. Thus, for a given radiotracer, selection of, and particle modification with, the proper chelator may be very difficult or even impossible.[15] Even when isotopes are stably

Received: September 12, 2014
Revised: December 16, 2014
Published: January 5, 2015

DOI: 10.1021/nl503522y
Nano Lett. 2015, 15, 864−868

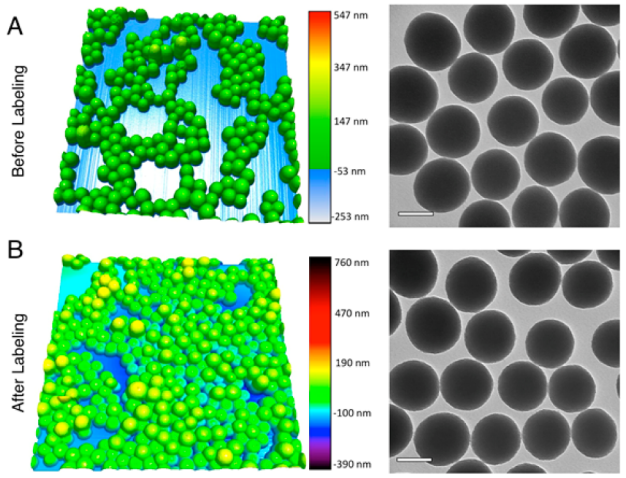

Figure 2. Pre- and postradiolabeling nanoparticle characterization. (A) Atomic force microscopy (AFM) and transmission electron microscopy (TEM) characterization of silica nanoparticles before radiolabeling. (B) AFM and TEM characterization of silica nanoparticles after radiolabeling with ^{68}Ga. The size and shape of the nanoparticles remains unchanged. Scale bars are 100 nm.

chelated during radiolabeling, introduction of the nanoparticle in vivo presents a new set of challenges. Transchelation by endogenous proteins or detachment of the surface-bound molecular chelators can strip the nanoparticles of their radiolabels, yielding images that do not reflect the true biodistribution.[16]

In response to the above-mentioned concerns, several chelator-free approaches to nanoparticle labeling have emerged and are the subject of a recent review.[15] These methods largely fall into three categories: inclusion of a trace amount of radioactive precursor during a typical nanoparticle synthesis (e.g., including a small amount of ^{64}Cu during synthesis of CuS nanoparticles),[17] entrapment of radioisotopes into sites capable of binding specific species (e.g., addition of ^{18}F to $NaYF_4$ nanoparticles, ^{64}Cu into porphysomes, and so forth),[18,19] and cation exchange replacing one (cold) cation present in a nanoparticle for a different radioactive (hot) cation (e.g., ^{153}Sm replacing Lu^{3+} or Y^{3+} in upconverting nanoparticles).[20] While these approaches eliminate the need for molecular chelators during nanoparticle radiolabeling, they remain restricted to specific isotopes, rather than being effective general platforms for many species.

A generalized method for producing nanoparticles that are capable of intrinsically binding a wide variety of radioisotopes without additional selective chelation molecules would be highly desirable. It would provide a "one stop shop" nanoparticle that can be radiolabeled for multiple applications without being individually modified with different chelators each time. To this end, we first identified some important properties shared between many common isotopes. The majority of medically relevant isotopes are chelated by electron donors (e.g., oxygen, sulfur, or nitrogen atoms) arranged in a symmetry that results in a stable coordination complex.[21] In this regard, it is reasonable to hypothesize that a chelator-free nanoparticle for intrinsic radiolabeling could be constructed by creating a nanoparticle with oxygen atoms arranged in a variety of symmetries. A prototypical example of a material meeting these requirements is amorphous silica, which has the benefits of well-established synthetic protocols and widespread use in biomedical applications.[22,23] Silica nanoparticles are known to bind heavy metal ions for environmental remediation.[24,25] Because silica nanoparticles are inexpensive and "generally recognized as safe" by the Food and Drug Administration, they

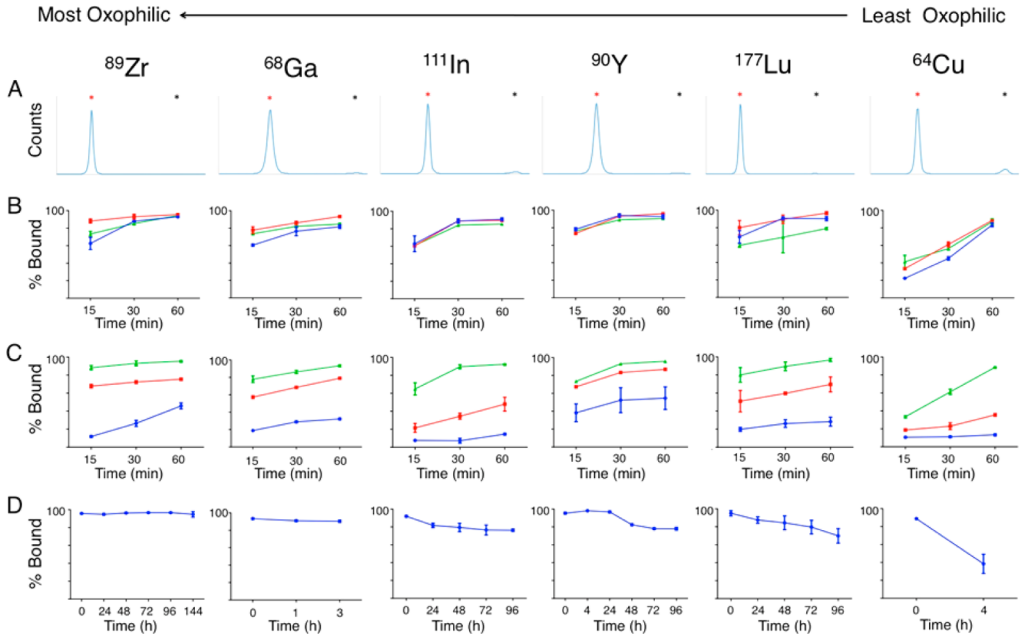

Figure 3. Radiolabeling and serum stability of silica nanoparticles. (A) Instant thin-layer chromatographs of radiolabeled silica nanoparticles. The red asterisk denotes the origin, where the nanoparticles remain, and the black asterisk denotes the solvent front, where the free activity would be located. Controls of buffer-only solutions (no particles) were ran with each condition with >95% signal at the free activity peak. (B) Percent radioisotope bound to silica nanoparticles as a function of time and pH. The blue, red, and green lines indicate radiolabeling at pH = 5.5, 7.3, and 8.8, respectively. (C) Percent radioisotope bound to silica nanoparticles as a function of time and temperature. The blue, red, and green lines indicate radiolabeling at 4, 37, and 70 °C, respectively. (D) Serum stability of silica nanoparticles radiolabeled at pH = 7.3 and 70 °C, then incubated in 50% FBS at 37 °C.

DOI: 10.1021/nl503522y
Nano Lett. 2015, 15, 864−868

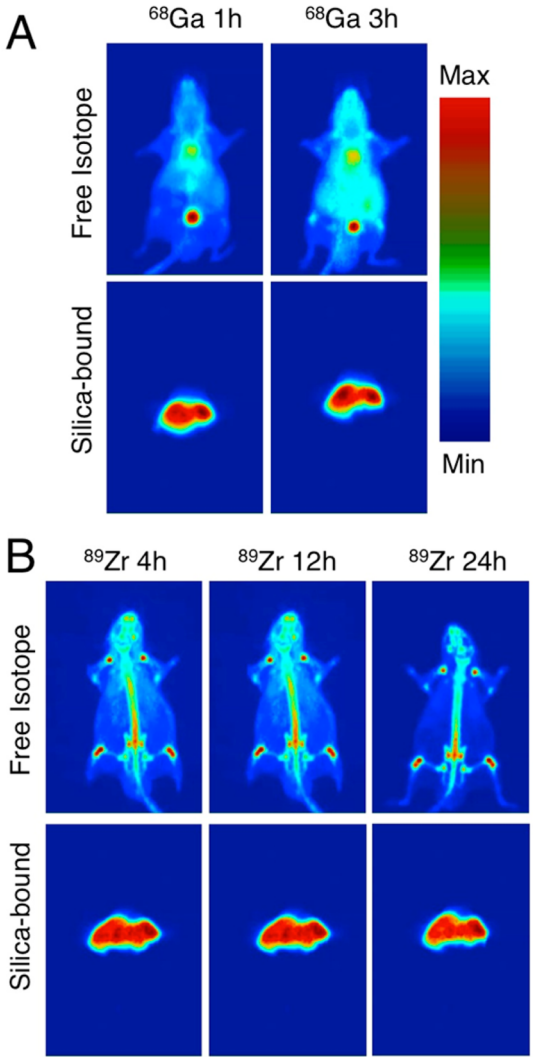

Figure 4. In vivo coronal PET maximum intensity projections (MIPs) of free and silica-bound radiotracers in athymic nude mice, 250–350 μCi (9.25–12.95 MBq) per injection. (A) MIPs of free (top) and silica-bound (bottom) ^{68}Ga at 1 and 3 h post injection. (B) MIPs of free (top) and silica-bound (bottom) ^{89}Zr at 4, 12, and 24 h post injection. The intrinsically labeled silica nanoparticles exhibit contrast in the reticuloendothelial system (liver, spleen), the known biodistribution of silica nanoparticles, whereas the free isotopes demonstrate an entirely different biodistribution. This stark contrast indicates that the silica nanoparticles remain intrinsically labeled in vivo.

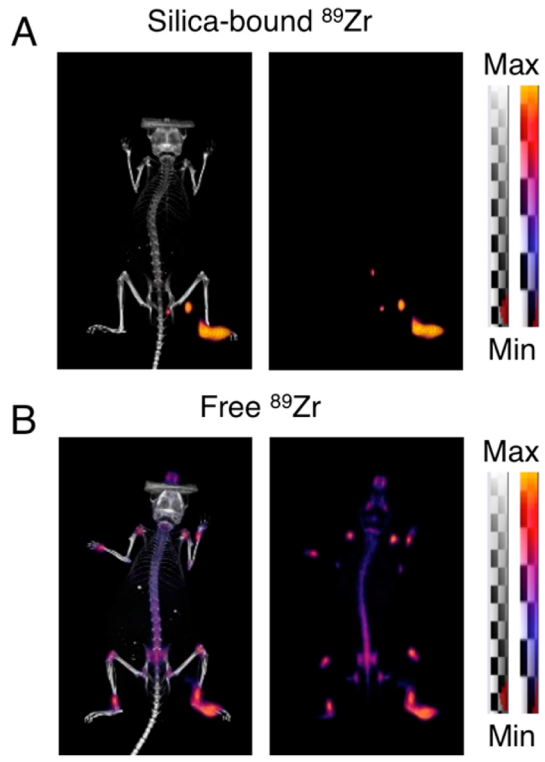

Figure 5. In vivo PET-CT (left) and PET-only (right) lymph node imaging after injection in the right rear paw of athymic nude mice. (A) Silica nanoparticles intrinsically labeled with ^{89}Zr 48 h post injection. (B) Free ^{89}Zr 48 h post injection. Images at earlier time points demonstrated the same trend, where the free ^{89}Zr did not accumulate in lymph nodes, while the intrinsically labeled silica nanoparticles progressively moved through the lymphatic system.

make for ideal substrates in a kitlike protocol for producing intrinsically labeled nanoparticles (Figure 1).[26]

We investigated the ability of amorphous silica nanoparticles to bind a variety of medically important radioisotopes with a range of half-lives and emissions. In particular, we explored the labeling efficiency of ^{68}Ga, ^{64}Cu, ^{89}Zr, ^{90}Y, ^{111}In, and ^{177}Lu under various temperatures, pH, and incubation times (Figure 3). ^{89}Zr was further investigated using silica nanoparticles that had been coated with polyethylene glycol. The 145 nm silica nanoparticles were synthesized according to a modified Stöber method,[22] washed three times in ethanol and then resuspended in buffered solutions at either pH = 5.7, 7.3, or 8.8 (see Supporting Information). The silica nanoparticles maintained a constant size and did not aggregate during this process (Figure 2). The radiochemical yield was assessed both by iTLC and centrifugal nanoparticle purification (Figure 3).

When the specific activity is 100 Ci/μmol, all isotopes tested demonstrate radiochemical yields of >99% (as measured by centrifugal nanoparticle purification) at pH = 7.3, 70 °C and incubation times less than or equal to 1 h. The radiochemical yield improves as temperature increases from 4 to 70 °C but does not vary significantly as a function of pH in the range investigated (pH = 5.7–8.8). Buffer without silica nanoparticles was used as a control for each condition to exclude the possibility of false-positive signals due to precipitate formation. Every isotope except ^{177}Lu shows >95% activity as free in solution, which is in agreement with previous reports.[27] Because ^{177}Lu exhibits >10% signal associated with precipitate formation in the buffer control, centrifugation and size exclusion filtration is necessary in the analysis of ^{177}Lu radiolabeling to ensure that false-positive signals from precipitates do not occur. Separating the particles from the supernatant shows that all of the radioactivity is associated with the nanoparticles, independent of temperature. Competitive chelation studies with ethylenediaminetetraacetic acid (EDTA) demonstrate that only samples incubated at 70 °C robustly retain the various isotopes. This suggests that the dominant influence of the temperature is in overcoming the activation energy required for stable radioisotope binding, rather than enabling delivery of the radioisotopes to binding sites (i.e., the process is reaction limited, not diffusion limited). This finding is supported by the observation that the silica nanoparticles are sufficiently porous to enable diffusion of the radioisotopes into

DOI: 10.1021/nl503522y
Nano Lett. 2015, 15, 864–868

the nanoparticle interior (Supporting Information Figure S1). While heating the particles to 70 °C precludes prelabeling attachment of temperature-sensitive targeting ligands such as antibodies, other targeting ligands that are stable at this temperature such as smaller peptides and aptamers may be used. Figure S2 demonstrates that PEGylation of the silica nanoparticles does not preclude ^{89}Zr binding. Therefore, attachment of moieties incompatible with the reported labeling procedure can be facilitated by first radiolabeling silica nanoparticles coated with functionalized polyethylene glycol, then performing straightforward postradiolabeling reactions. The nanoparticle size and zeta potential before and after radiolabeling are given in Supporting Information Table S1.

With these established protocols for achieving chelator-free high specific activities, the stability of the silica nanoparticles under physiological conditions was examined. The serum stability of each isotope was investigated in 50% fetal bovine serum at 37 °C over time periods appropriate to each isotope's half-life. All isotopes were stably retained within the silica nanoparticles except for ^{64}Cu. In the case of copper, 50% of the bound isotope leached into the serum after 4 h. Because the operating principle of intrinsic labeling with silica nanoparticles is the affinity each isotope has for the oxygen-rich matrix, it is unsurprising that copper is most weakly retained because it is the least oxophilic of the isotopes tested. In fact, the trend in serum stability of the intrinsically labeled silica demonstrated excellent correlation with the oxophilicity (i.e., hardness) of the ions.[28] The marked decrease in the serum stability of ^{64}Cu can be further attributed to proteins present in the serum that actively chelate copper ions, resulting in pronounced transchelation effects.[29]

The stability and biodistribution of ^{68}Ga- and ^{89}Zr-labeled silica nanoparticles was also investigated in vivo. These isotopes are particularly interesting because of their increasing clinical importance in PET imaging, disparity in half-life, and excellent serum stability.[30,31] Because nanoparticles are known to generally accumulate in the reticuloendothelial system in amounts well exceeding 90% of the injected dose,[6] short-lived isotopes like ^{68}Ga are attractive in minimizing the cross-dose to healthy organs while still enabling whole-body cancer imaging. Alternatively, because some nanoparticle formulations remain in circulation for extended periods and most nanoparticle clearance studies extend for weeks or longer, long-lived isotopes like ^{89}Zr are essential for investigating the biological response to nanoparticle administration. An additional benefit of studying these two isotopes is that the biodistribution of free ^{68}Ga and ^{89}Zr is easily distinguished in the biodistribution of nanoparticles in that they do not preferentially residualize in the liver and spleen (Figure 4a), which is in contrast to other isotopes like ^{64}Cu that naturally accumulate in the liver. Male athymic nude mice (8−10 weeks old, n = 3) were injected with 250−350 μCi (9.25−12.95 MBq) of either free ^{68}Ga or ^{89}Zr while another set was injected with ^{68}Ga- or ^{89}Zr-silica nanoparticles (10 nM) in 100 μL of 10 mM pH = 7.3 2-(N-morpholino)-ethanesulfonic acid solution via the lateral tail vein. The nanoparticle-bound isotopes demonstrated the known biodistribution of silica nanoparticles and remained localized in the liver and spleen for the entire period investigated (3 h for ^{68}Ga, 24 h for ^{89}Zr, n = 3 for each) (Figure 4b).[32] The stark contrast between the free and nanoparticle-bound biodistributions demonstrates that the silica nanoparticles stably retain the isotopes in vivo (Supporting Information Figure S3).

Because silica serves as a robust platform for binding radioisotopes and retaining them in vivo, the nanoprobes generated by this kitlike radiolabeling protocol should be immediately useful in the many known biomedical applications of nanoparticles. As a proof of concept, we attempted to use these nanoparticles for lymph node imaging, a clinically important application where nanoparticles demonstrate great promise.[33] We injected either free ^{89}Zr or nanoparticle-bound ^{89}Zr (n = 3 per condition, 3.7−5.5 MBq, 20−30 μL) into the footpad of male athymic nude mice (see Supporting Information for methods) and performed whole-body PET-CT scans. In all cases, the nanoparticle-bound radioisotopes enabled robust detection of local lymph nodes while the free radioisotope controls did not (Figure 5, Supporting Information Figure S4).

In summary, this work has established the ability of amorphous silica nanoparticles to intrinsically bind a wide variety of radioisotopes without the need for additional chelators. The in vivo stability demonstrated herein validates the use of these nanoparticles in well-established and future biomedical applications,[34,35] and it is foreseeable that other particles could be coated with silica for facile and highly efficient radiolabeling.[36] Moreover, our findings warrant careful evaluation of radiolabeling procedures for similar nanoparticles that utilize molecular chelators in order to prevent misinterpretation of labeling mechanisms and efficiency.

■ ASSOCIATED CONTENT

Supporting Information

Table of nanoparticle characterization pre- and post-radiolabeling, AFM-characterization of SNP pore sizes, influence of PEGylation on intrinsic radiolabeling, classical biodistribution studies of ^{68}Ga- and ^{89}Zr-radiolabeled SNPs, lymph node time course imaging, and detailed methods. This material is available free of charge via the Internet at http://pubs.acs.org.

■ AUTHOR INFORMATION

Corresponding Authors

*E-mail: kircherm@mskcc.org.
*E-mail: grimmj@mskcc.org.

Author Contributions

#T.M.S. and M.A.W. contributed equally to this work. M.A.W. and S.H. synthesized and characterized the silica nanoparticles. T.M.S. completed all radiolabeling and radiochemical characterization, along with animal work and imaging. V.A.L. assisted in animal work and imaging. C.M.D., M.F.K., and J.G. supervised the project. All authors contributed discussions on the project. The manuscript was written by M.A.W. and T.M.S. and edited by C.M.D., M.F.K. and J.G.

Notes

The authors declare the following competing financial interest(s): The authors Shaffer, Wall, Harmsen, Kircher, and Grimm have filed a provisional patent application regarding the content of the manuscript.

■ ACKNOWLEDGMENTS

The authors thank K. Pillarsetty for expert radiochemical assistance. The Australian Nuclear Science and Technology Organisation (ANSTO) is acknowledged for their generous provision of a research-grade gallium-68 generator and purification system. This work was supported by the following grants: NIH R01EB014944 and R01CA183953 (to J.G.). NIH

DOI: 10.1021/nl503522y
Nano Lett. 2015, 15, 864−868

R01 EB017748 and NIH K08 CA163961 (to M.F.K.). MSKCC Technology Development Fund (M.F.K.). T.M.S. and M.A.W. are funded by a National Science Foundation Integrative Graduate Education and Research Traineeship Grant (NSF, IGERT 0965983 at Hunter College). M.F.K. is a Damon Runyon-Rachleff Innovator supported (in part) by the Damon Runyon Cancer Research Foundation (DRR-29-14). Technical services provided by the MSKCC Small-Animal Imaging Core Facility were supported in part by the MSKCC NIH Core Grant (P30-CA008748) and NIH Shared Instrumentation Grant No 1 S10 OD016207-01, which provided funding support for the purchase of the Inveon PET/CT. Funding for the AMF was provided by a Core Support Grant of MSKCC's Experimental Therapeutics Center (to J.G. as Co-PI).

REFERENCES

(1) Kircher, M. F.; Willmann, J. K. Molecular Body Imaging: MRI, CT and US. Part II - Applications. *Radiology* **2012**, *264* (2), 349−368.
(2) Karabeber, H.; Huang, R.; Iacono, P.; Samii, J.; Pitter, K.; Holland, E. C.; Kircher, M. F. Guiding Brain Tumor Resection using Surface-Enhanced Raman Scattering Nanoparticles and a Hand-Held Raman Scanner. *ACS Nano.* **2014**, *8* (10), 9755−9766.
(3) Lee, J. E.; Lee, N.; Kim, T.; Kim, J.; Hyeon, T. *Acc. Chem. Res.* **2011**, *44* (10), 893−902.
(4) Kaittanis, C.; T, M. S.; Thorek, D. L.; Grimm, J. *Crit. Rev. Oncog.* **2014**, *19*, 143−176.
(5) Otsuka, H.; Nagasaki, Y.; Kataoka, K. *Adv. Drug Deliver Rev.* **2003**, *55* (3), 403−419.
(6) Moghimi, S. M.; Hunter, A. C.; Murray, J. C. *Pharmacol Rev.* **2001**, *53* (2), 283−318.
(7) Kim, J.; Kim, H. S.; Lee, N.; Kim, T.; Kim, H.; Yu, T.; Song, I. C.; Moon, W. K.; Hyeon, T. *Angew. Chem., Int. Ed.* **2008**, *47* (44), 8438−8441.
(8) Decuzzi, P.; Pasqualini, R.; Arap, W.; Ferrari, M. *Pharm. Res.* **2009**, *26* (1), 235−243.
(9) Perrault, S. D.; Walkey, C.; Jennings, T.; Fischer, H. C.; Chan, W. C. W. *Nano Lett.* **2009**, *9* (5), 1909−1915.
(10) Meng, H.; Xue, M.; Xia, T.; Ji, Z. X.; Tarn, D. Y.; Zink, J. I.; Nel, A. E. *ACS Nano* **2011**, *5* (5), 4131−4144.
(11) Kumar, R.; Roy, I.; Ohulchanskky, T. Y.; Vathy, L. A.; Bergey, E. J.; Sajjad, M.; Prasad, P. N. *ACS Nano* **2010**, *4* (2), 699−708.
(12) de Barros, A. B.; Tsourkas, A.; Saboury, B.; Cardoso, V. N.; Alavi, A. *EJNMMI Res.* **2012**, *2* (1), 39.
(13) Thorek, D. L. J.; Ulmert, D.; Diop, N. F. M.; Lupu, M. E.; Doran, M. G.; Huang, R. M.; Abou, D. S.; Larson, S. M.; Grimm, J. *Nat. Commun.* **2014**, *5*, 3097.
(14) Liu, S. *Adv. Drug Delivery Rev.* **2008**, *60* (12), 1347−1370.
(15) Goel, S.; Chen, F.; Ehlerding, E. B.; Cai, W. *Small* **2014**, *10*, 3825−3830.
(16) Boswell, C. A.; Sun, X. K.; Niu, W. J.; Weisman, G. R.; Wong, E. H.; Rheingold, A. L.; Anderson, C. J. *J. Med. Chem.* **2004**, *47* (6), 1465−1474.
(17) Zhou, M.; Zhang, R.; Huang, M. A.; Lu, W.; Song, S. L.; Melancon, M. P.; Tian, M.; Liang, D.; Li, C. *J. Am. Chem. Soc.* **2010**, *132* (43), 15351−15358.
(18) Sun, Y.; Yu, M. X.; Liang, S.; Zhang, Y. J.; Li, C. G.; Mou, T. T.; Yang, W. J.; Zhang, X. Z.; Li, B. A.; Huang, C. H.; Li, F. Y. *Biomaterials* **2011**, *32* (11), 2999−3007.
(19) Liu, T. W.; MacDonald, T. D.; Shi, J. Y.; Wilson, B. C.; Zheng, G. *Angew. Chem., Int. Ed.* **2012**, *51* (52), 13128−13131.
(20) Sun, Y.; Liu, Q.; Peng, J. J.; Feng, W.; Zhang, Y. J.; Yang, P. Y.; Li, F. Y. *Biomaterials* **2013**, *34* (9), 2289−2295.
(21) Wadas, T. J.; Wong, E. H.; Weisman, G. R.; Anderson, C. J. *Chem. Rev.* **2010**, *110* (5), 2858−2902.
(22) Stöber, W.; Fink, A.; Bohn, E. *J. Colloid Interface Sci.* **1968**, *26* (1), 62.
(23) Barik, T. K.; Sahu, B.; Swain, V. *Parasitol. Res.* **2008**, *103* (2), 253−8.
(24) Yang, X. F.; Shen, Z. G.; Zhang, B.; Yang, J. P.; Hong, W. X.; Zhuang, Z. X.; Liu, J. J. *Chemosphere* **2013**, *90* (2), 653−656.
(25) Burke, A. M.; Hanrahan, J. P.; Healy, D. A.; Sodeau, J. R.; Holmes, J. D.; Morris, M. A. *J. Hazard Mater.* **2009**, *164* (1), 229−234.
(26) Rosenholm, J. M.; Mamaeva, V.; Sahlgren, C.; Linden, M. *Nanomedicine* **2012**, *7* (1), 111−120.
(27) Boros, E. B.; A, M.; Josephson, L.; Vasdev, N.; Holland, J. P. *Chem. Sci.* **2015**, *6* (1), 225−236.
(28) Kinraide, T. B.; Yermiyahu, U. *J. Inorg. Biochem* **2007**, *101* (9), 1201−1213.
(29) Boal, A. K.; Rosenzweig, A. C. *Chem. Rev.* **2009**, *109* (10), 4760−4779.
(30) Velikyan, I. *Theranostics* **2013**, *4* (1), 47−80.
(31) Fischer, G.; Seibold, U.; Schirrmacher, R.; Wangler, B.; Wangler, C. *Molecules* **2013**, *18* (6), 6469−6490.
(32) van Schooneveld, M. M.; Vucic, E.; Koole, R.; Zhou, Y.; Stocks, J.; Cormode, D. P.; Tang, C. Y.; Gordon, R. E.; Nicolay, K.; Meijerink, A.; Fayad, Z. A.; Mulder, W. J. M. *Nano Lett.* **2008**, *8* (8), 2517−2525.
(33) Harisinghani, M. G.; Barentsz, J.; Hahn, P. F.; Deserno, W. M.; Tabatabaei, S.; van de Kaa, C. H.; de la Rosette, J.; Weissleder, R. *New Engl J. Med.* **2003**, *348* (25), 2491−U5.
(34) Jha, P.; Golovko, D.; Bains, S.; Hostetter, D.; Meier, R.; Wendland, M. F.; Daldrup-Link, H. E. *Cancer Res.* **2010**, *70* (15), 6109−6113.
(35) Thakor, A. S.; Gambhir, S. S. *Ca-Cancer J. Clin.* **2013**, *63* (6), 395−418.
(36) Thakor, A. S.; Luong, R.; Paulmurugan, R.; Lin, F. I.; Kempen, P.; Zavaleta, C.; Chu, P.; Massoud, T. F.; Sinclair, R.; Gambhir, S. S. *Sci. Transl Med.* **2011**, *3* (79), 79ra33.

DOI: 10.1021/nl503522y
Nano Lett. 2015, 15, 864−868